

Spectral and atmospheric characterisation of a new benchmark brown dwarf HD 13724 B ★ ★

E. L. Rickman¹, D. Ségransan¹, J. Hagelberg¹, J.-L. Beuzit², A. Cheetham¹, J.-B. Delisle¹, T. Forveille³, S. Udry¹

¹ Département d'astronomie de l'Université de Genève, 51 ch. des Maillettes Sauverny, 1290 Versoix, Switzerland
e-mail: emily.rickman@unige.ch

² Aix Marseille Univ., CNRS, CNES, LAM, Marseille, France

³ Univ. Grenoble Alpes, CNRS, IPAG, 38000 Grenoble, France

Received ; accepted

ABSTRACT

Context. HD 13724 is a nearby solar-type star at 43.48 ± 0.06 pc hosting a long-period low-mass brown dwarf detected with the CORALIE echelle spectrograph as part of the historical CORALIE radial-velocity search for extra-solar planets. The companion has a minimum mass of $26.77^{+4.4}_{-2.2} M_{\text{Jup}}$ and an expected semi-major axis of ~ 240 mas making it a suitable target for further characterisation with high-contrast imaging, in particular to measure its inclination, mass, and spectrum and thus establish its substellar nature.

Aims. Using high-contrast imaging with the SPHERE instrument on the Very Large Telescope (VLT), we are able to directly image a brown dwarf companion to HD 13724 and obtain a low-resolution spectrum.

Methods. We combine the radial-velocity measurements of CORALIE and HARPS taken over two decades and high contrast imaging from SPHERE to obtain a dynamical mass estimate. From the SPHERE data we obtain a low resolution spectrum of the companion from Y to J band, as well as photometric measurements from IRDIS in the J , H and K bands.

Results. Using high-contrast imaging with the SPHERE instrument at the VLT, we report the first images of a brown dwarf companion to the host star HD 13724. It has an angular separation of 175.6 ± 4.5 mas and H -band contrast of 10.61 ± 0.16 mag and, using the age estimate of the star to be ~ 1 Gyr, gives an isochronal mass estimate of $\sim 44 M_{\text{Jup}}$. By combining radial-velocity and imaging data we also obtain a dynamical mass of $50.5^{+3.3}_{-3.5} M_{\text{Jup}}$. Through fitting an atmospheric model, we estimate a surface gravity of $\log g = 5.5$ and an effective temperature of 1000 K. A comparison of its spectrum with observed T dwarfs estimates a spectral type of T4 or T4.5, with a T4 object providing the best fit.

Key words. planetary systems - binaries: visual - techniques: radial velocities, high angular resolution - stars: brown dwarfs, general - HD 13724

1. Introduction

Evolutionary models of brown dwarfs are plagued by a lack of observational constraints in addition to model degeneracies. The complex molecular chemistry of their atmospheres leaves a relatively wide parameter space for models to span. For this reason, the detection of brown dwarfs are vital to test their complex atmospheres, as well as the structure and evolution of these substellar objects (Baraffe et al. 2003, 2015). Furthermore, it is crucial to characterise brown dwarfs that are orbiting stars, where the age of the system can be constrained unlike field brown dwarfs. In addition, brown dwarfs orbiting stars allows us to monitor the radial-velocity (RV) of these systems allowing us to place constraints on their dynamical masses over time (Boden et al. 2006).

With over 20 years worth of RV measurements from the CORALIE survey for extrasolar planets (Udry et al. 2000),

HD 13724 has been previously identified as a promising candidate for observational follow-up with direct imaging (Rickman et al. 2019) due to its minimum mass ($26.77^{+4.4}_{-2.2} M_{\text{Jup}}$) and expected semi-major axis (~ 240 mas) that is calculated from the orbital period measured by RV measurements to date.

The CORALIE RV survey is a volume-limited sample of 1647 main sequence stars from F8 down to K0 located within 50 pc of the Sun. With such a long base line of observations, it allows us to detect massive giant planets at separations larger than 5 AU. This in turn identifies golden targets for direct imaging, as such companions are rare and are very difficult to search for blindly. Selecting long-period candidates to image from RV surveys has proven to be valuable (see Cheetham et al. (2018); Peretti et al. (2019)).

RV measurements provide a lower limit on the measured masses due to the unknown orbital inclination. Therefore directly imaging long-period RV candidates allows us to break that degeneracy and provide constraints on the dynamical mass of the companion.

Not only does combining these two detection techniques allow us to start filling in a largely unexplored parameters space, but through combining RV and direct imaging data we can now expect to dynamically measure the mass of such companions. By constraining the mass, we are able to place additional constraints on the evolution of the companion, both in terms of tem-

* Based on observations collected with SPHERE mounted on the VLT at Paranal Observatory (ESO, Chile) under programmes 0102.C-0236(A) (PI: Rickman) and 0104.C-0702(B) (PI: Rickman) as well as observations collected with the CORALIE spectrograph mounted on the 1.2 m Swiss telescope at La Silla Observatory and with the HARPS spectrograph on the ESO 3.6 m telescope at La Silla (ESO, Chile).

** The radial-velocity measurements, reduced images and additional data products discussed in this paper are available on the DACE web platform at <https://dace.unige.ch/>.

perature and atmospheric composition (for example, see Maire et al. (2016a); Vigan et al. (2016)).

To date, individual dynamical masses from combining radial velocity and imaging measurements are known for only a handful of brown dwarfs (Thalmann et al. 2009; Sahlmann et al. 2011; Crepp et al. 2012, 2014, 2016; Dupuy & Liu 2017; Peretti et al. 2019; Bowler et al. 2018; Cheetham et al. 2018; Brandt et al. 2019; Maire et al. 2019), therefore any new detections contributes greatly to brown dwarf models in addition to providing important analogues for the characterisation of exoplanets. This forms part of a larger effort to determine the giant planet upper mass limit and lower mass limit for brown dwarfs, especially in the $\sim 20 M_{\text{Jup}} - 40 M_{\text{Jup}}$ range where there is a dearth in the number of companions observed (Sahlmann et al. 2011). Detecting brown dwarfs in this parameter space can help us understand the formation of these objects, whether they formed via gravitational instability like binary systems or via core accretion like planets. This is crucial in understanding the formation processes of such systems and defining the boundary between massive planets and low-mass brown dwarfs.

To determine the mass of an imaged brown dwarf companion, the key parameter for the evolution of substellar objects, we usually rely on evolutionary models (Marley et al. 1996; Baraffe et al. 2003; Allard et al. 2012; Morley et al. 2012). These models still need to be tested and properly calibrated through observations. The discovery of benchmark sources provides a powerful and critical tool in achieving this. As we move toward imaging smaller and smaller objects it is important to use these objects as a laboratory to test theoretical atmospheric models.

Typically direct imaging is more favourable around young stars where any companion will still be bright and hot and therefore easier to detect. Whereas the RV method typically favours older stars where the RV signal is not too contaminated from variability caused by stellar activity in young and active stars. Consequently, combining these two techniques allows us to not only probe a mass-separation parameter space that is largely unexplored, but also bridge the gap between younger and older companion candidates.

We report here the first images and low resolution spectrum of the benchmark brown dwarf HD 13724 B. In addition, we extend the time baseline of the RV observations. When combined with the imaging data, this allows constraints to be placed on the mass and orbital parameters of the brown dwarf companion. Thanks to the high precision of the RV data and the number of points, the minimum mass is well constrained and only a few astrometric points from high-contrast imaging provides a high-precision orbit and dynamical mass.

The paper is organised as follows. The host star's properties are summarised in Sect. 2. In Sect. 3 we summarise the observations and data analysis procedures for the RV and high-contrast imaging data. In Sect. 4 we present the results of the imaging data analysis and derived companion properties, as well as giving an overview of the results from the combined orbital fitting. The results are discussed in Sect. 5 with some concluding remarks.

2. Stellar Characterisation

The observed and inferred stellar parameters for HD 13724 are summarised in Table 1. The spectral type, V band magnitude and colour index is taken from the HIPPARCOS and Tycho catalogues (Hoeg et al. 1997; Perryman et al. 1997), while the astrometric parallax (π) and luminosity is taken from the second *Gaia* data release (Gaia Collaboration et al. 2018). The effective

Table 1. Stellar Parameters of HD 13724

Parameters	units	HD 13724
Spectral Type ^(a)		G3/G5V
V ^(a)		7.89
$B - V$ ^(a)		0.667
π ^(b)	[mas]	23.0 ± 0.03
M_v		4.70
T_{Gaia} ^(b)	[K]	$5775.33^{+49.67}_{-74.33}$
$\log g$	[cgs]	4.44 ± 0.07
[Fe/H]	[dex]	0.23 ± 0.02
$v \sin i$ ^(c)	[km s ⁻¹]	3.025
M_*	[M _⊙]	1.14 ± 0.06
L_{Gaia} ^(b)	[L _⊙]	$1.14^{+0.001}_{-0.002}$
R_{Gaia} ^(b)	[R _⊙]	1.07 ± 0.02
$\log R'_{HK}$ ^(c)		-4.76 ± 0.003
P_{rot}	[days]	20.2 ± 1.2
Age	[Gyr]	1.04 ± 0.88

Notes. ^(a) Parameters taken from HIPPARCOS and Tycho (Perryman et al. 1997; Hoeg et al. 1997) ^(b) Parallaxes taken from *Gaia* data release 2 (Gaia Collaboration et al. 2018) ^(c) Parameters derived using CORALIE CCF.

temperature, gravity and metallicities are derived using the same spectroscopic methods as applied in Santos et al. (2013), whilst the $v \sin i$ is computed using the calibration of CORALIE's Cross Correlation Function (CCF) (Santos et al. 2001; Marmier 2014).

The mean chromospheric activity index - $\log(R'_{HK})$ - is computed by co-adding the corresponding CORALIE spectra to improve the signal-to-noise ratio which allows us to measure the Ca II re-emission at $\lambda = 3933.66\text{\AA}$. We derived an estimate of the rotational period of the star from the mean $\log(R'_{HK})$ activity index using the calibration of Mamajek & Hillenbrand (2008).

The stellar radius and uncertainties are derived from the *Gaia* luminosities and the effective temperatures are obtained from the spectroscopic analysis. A systematic error of 50 K was quadratically added to the effective temperature error bars and propagated in the radius uncertainties.

The mass and age of HD 13724, as well as the uncertainties, were derived using the Geneva stellar evolution modes (Ekström et al. 2012; Georgy et al. 2013). The interpolation in the model grid was made through a Bayesian formalism using observational Gaussian priors on T_{eff} , M_v , $\log g$ and [Fe/H] (Marmier 2014).

3. Observations and Data Reduction

RV and direct imaging observations were combined to constrain the orbit of HD 13724 B. The extensive orbital coverage of the RV time series allows us to constrain HD 13724 B's orbital parameters well. Combined with several direct imaging observations we are able to derive the orbital inclination i and thus the companion's mass. In addition, the SPHERE high-contrast IRDIS observations provides six narrow band-width photometric measurements in the *J*, *H* and *K* bands and IFS observations

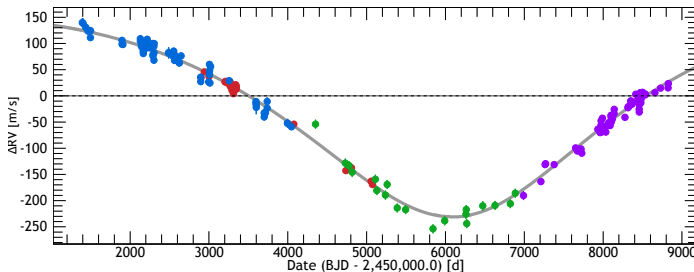


Fig. 1. HD13724 RV measurements as a function of Julian Dates obtained with CORALIE-98 (blue), CORALIE-07 (green) and CORALIE-14 (purple). The HARPS-03 data are shown in red. The best single-planet Keplerian model is represented as a black curve.

allows us to obtain a low-resolution spectrum of the brown dwarf companion in the $Y - J$ bands.

3.1. Radial Velocities

HD 13724 has been observed since August 1999 with the CORALIE spectrograph (Queloz et al. 2000) installed on the 1.2m EULER Swiss telescope at La Silla observatory (Chile) and HARPS (Mayor et al. 2003) on the ESO/3.6 m telescope to obtain radial-velocities.

The RV data analysis presented in this paper was accomplished using a set of online tools hosted by the Data & Analysis Center for Exoplanets (DACE)¹, which performs a Keplerian fit to the data as described in Delisle et al. (2016). The 179 measurements obtained between August 1999 and December 2019 are shown in Fig. 1 with the corresponding Keplerian model.

Since Rickman et al. (2019) we have obtained five more RV measurements over ~ 10 months. We have also added 4 historical and low precision (~ 300 m/s) CORAVEL measurements to increase the overall time span of the RV measurements by 10 years and to provide an upper bound constraint on the minimum mass of the companion. The RV data products presented in this paper are available at DACE with the new orbital parameters shown in Table 3. The full description of the RV data is outlined in Rickman et al. (2019).

3.2. SPHERE high-contrast imaging

HD 13724 was observed with SPHERE, the extreme adaptive optics system at the VLT (Beuzit et al. 2019) on 2018-08-18, 2019-10-12 and 2019-10-18. Observations were taken using the IRDIFS mode, which allows the Integral Field Spectrograph (IFS; Mesa et al. (2015)) and the InfraRed Dual-Band Imager and Spectrograph (IRDIS; Dohlen et al. (2008)) modules to be used simultaneously. The IFS data cover a range of wavelengths from $Y - J$ (0.96–1.34 μ m, spectral resolution $R \sim 54$). The IRDIS data were taken in the dual-band imaging mode (Vigan et al. 2010) using the $H2$ and $H3$ filters ($\lambda_{H2} = 1.58888 \mu\text{m}$, $\lambda_{H3} = 1.6671 \mu\text{m}$), as well as using the $J2$ and $J3$ filters ($\lambda_{J2} = 1.190 \mu\text{m}$, $\lambda_{J3} = 1.273 \mu\text{m}$) and the $K1$ and $K2$ band filters ($\lambda_{K1} = 2.110 \mu\text{m}$ and $\lambda_{K2} = 2.251 \mu\text{m}$), such that the $J2$, $H3$ and $K2$ bands align with methane absorption bands.

The observing sequence consisted of long-exposure images taken with an apodized Lyot coronagraph (Soummer et al. 2003). To measure the position of the star behind the coronograph, sev-

eral exposures were taken with a sinusoidal modulation applied to the deformable mirror (to generate satellite spots around the star) at the beginning and at the end of the sequence. To estimate the stellar flux and the shape of the point-spread function (PSF) during the sequence, several short exposure images were taken with the star moved from behind the coronagraph, and using a neutral-density (ND) filter with a $\sim 10\%$ transmission², also at the beginning and end of the sequence. In addition, several long-exposure sky frames were taken to estimate the background flux and help identify bad pixels on the detector.

The SPHERE Data Reduction and Handling pipeline (Pavlov et al. 2008) was used to perform the wavelength extraction for the IFS data, turning the full-frame images of the lenslet spectra into image cubes.

The remainder of the data reduction and analysis was completed using the Geneva Reduction and Analysis Pipeline for High-contrast Imaging of planetary Companions (GRAPHIC) (Hagelberg et al. 2016). The data were first sky subtracted, flat fielded, cleaned of bad pixels, and corrected for distortion (following Maire et al. (2016b)). We then run a principal component analysis (PCA) PSF subtraction algorithm (Soummer et al. 2012; Amara & Quanz 2012) which is run separately for images at each wavelength channel and for each IRDIS channel. The resulting frames were derotated and median combined to produce a final PSF-subtracted image.

In addition to this, we performed a spectral differential imaging (SDI) reduction for both the IFS and IRDIS datasets. The same PCA algorithm was then performed on the resulting images. The resulting PCA-reduced and SDI IRDIS and IFS images are shown in Fig. 2.

4. Results

4.1. Astrometry and Photometry

The relative astrometry and photometry were calculated using a negative fake planet injection on the images (Bonnefoy et al. 2011). An initial Nelder-Mead minimisation routine (Gao & Han 2012) was used to find a first order estimation of the separation (in pixels), position angle (in degrees) and contrast ratio between the star and the companion. We then fit over a 3D grid of parameters for the position and the flux of the fake negative PSF to minimise the residuals and to numerically derive the χ^2 with the associated 68.27% confidence interval. We then correct for the pixel scale and true north angle given in Maire et al. (2016b). The resulting parameters are listed in Table 2.

The IFS data consists of data taken in the wavelength range 0.96–1.34 μ m that is split into 39 wavelength channels, giving 39 images across the wavelength range. Because of the low signal-to-noise ratio in some of the spectral channels, we use a different approach to measure the companion flux. For the IFS data, we perform a fit for the separation and position angle using the negative fake planet injection using a stacked image across all of the wavelength channels in order to have a high signal-to-noise ratio for the companion fit. Using this fitted position on the image, we then fit for the contrast ratio between the companion and the star at each wavelength channel in order to extract the spectrum.

² The corrections for the ND filter transmission are done using the ND filter curves given at <https://www.eso.org/sci/facilities/paranal/instruments/sphere/inst-filters.html>

¹ The DACE platform is available at <https://dace.unige.ch> where the online tools to analyse RV data can be found in the section Observations->Radial Velocities.

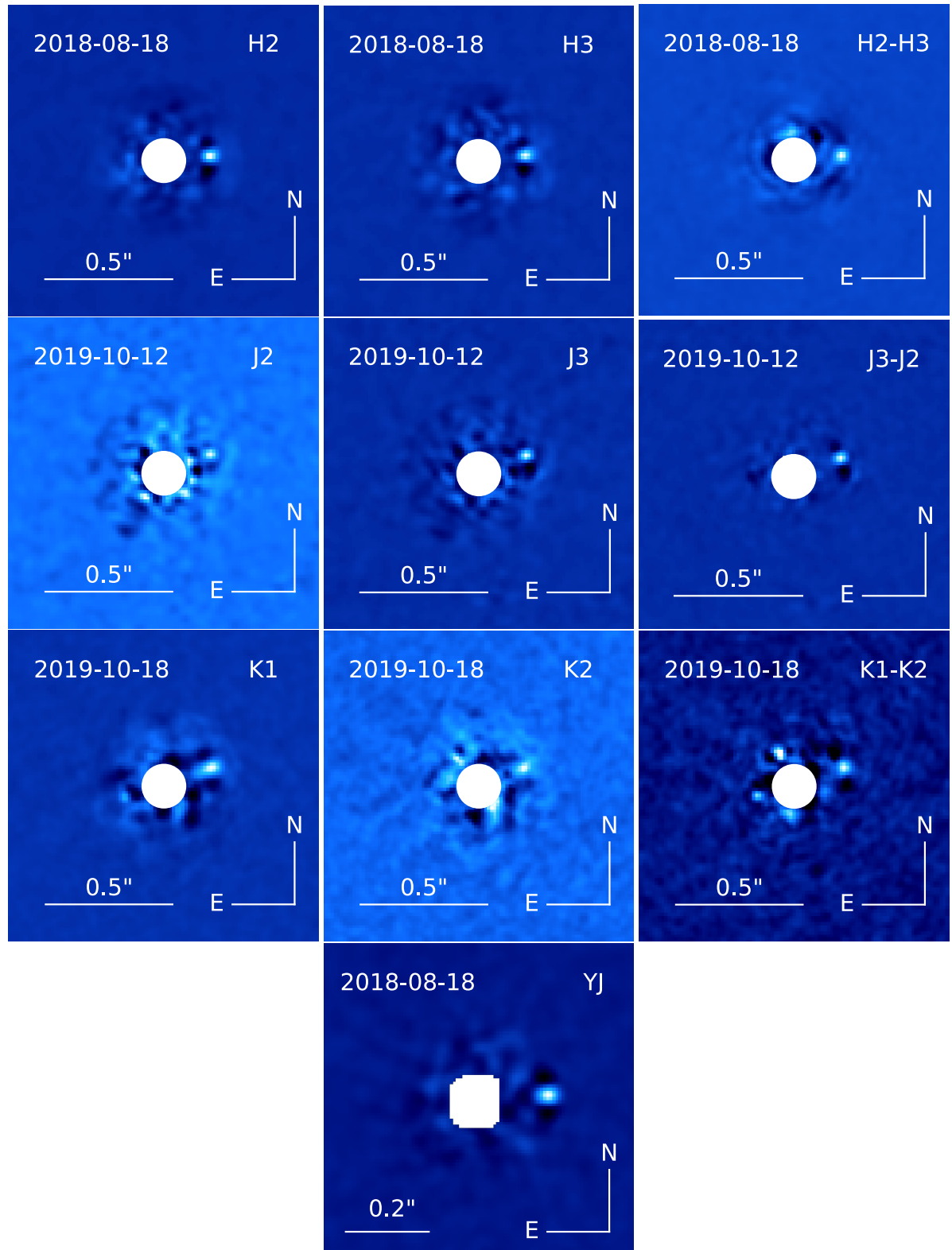


Fig. 2. IRDIS and IFS images of HD 13724. The star is masked by the white circle. We also show a weighted combination of the IFS SDI image. Each IFS wavelength channel was weighted by the average flux predicted by the best-fitting BT-Settl model (Allard et al. 2012).

4.2. Orbit determination and dynamical mass

To constrain the orbital parameters of the brown dwarf, we performed a combined fit to the RV and direct-imaging data. For this we used the IRDIS $H2$, $H3$, $J2$, $J3$, $K1$ and $K2$ astrome-

try $\{\rho(t), \theta(t)\}$ where $\rho(t)$ is the observed separation in mas and $\theta(t)$ is the position angle in deg (see Table 4). This allows us to place constraints on the period, eccentricity and inclination of the system.

Table 2. The measured relative astrometry and photometry of HD 13724 B from the SPHERE observations.

Instrument	Filter	Date	BJD ^(a)	ρ (mas)	θ (deg)	Contrast (mag)
IRDIS	H2	2018-08-18	58349.29438	175.61 ± 4.45	272.15 ± 1.06	10.61 ± 0.16
IRDIS	H3	2018-08-18	58349.29438	178.85 ± 4.56	272.50 ± 1.71	11.34 ± 0.32
IRDIS	H2-H3	2018-08-18	58349.29438	177.70 ± 4.41	270.75 ± 1.76	11.71 ± 0.35
IRDIS	J2	2019-10-12	58768.16564	179.9 ± 12.69	289.92 ± 2.49	11.50 ± 0.40
IRDIS	J3	2019-10-12	58768.16564	188.90 ± 4.98	288.75 ± 1.05	10.37 ± 0.04
IRDIS	J3-J2	2019-10-12	58768.16564	187.59 ± 1.60	288.25 ± 0.58	10.82 ± 0.09
IRDIS	K1	2019-10-18	58774.20206	190.55 ± 9.05	288.75 ± 1.51	10.29 ± 0.18
IRDIS	K2	2019-10-18	58774.20206	192.12 ± 15.84	288.75 ± 2.52	11.10 ± 0.46
IRDIS	K1-K2	2019-10-18	58774.20206	200.32 ± 16.15	288.58 ± 2.62	11.15 ± 0.43

Notes. ^(a) The date is expressed as BJD-2400000.0.

Due to two major upgrades to CORALIE in June 2007 (Ségransan et al. 2010) and in November 2014, we consider CORALIE as three different instruments, corresponding to the different upgrades: the original CORALIE as CORALIE-98 (C98), the first upgrade as CORALIE-07 (C07) and the latest upgrade as CORALIE-14 (C14).

The observed RV signal was modelled with a single Keplerian and five RV offsets (corresponding to one offset for each RV instrument). HARPS-03 was chosen as the reference instrument while RV offsets were adjusted between CORAVEL, CORALIE-98, CORALIE-07 and CORALIE-14 and HARPS-03 which were marginalised over.

A linear correlation is observed between the H_{α} activity index time series and the observed radial velocities which allow us to carry out a first order detrending of the observed RV measurements using a linear scale factor between the H_{α} index time series and the modelled RVs (Delisle et al. 2018). A RV nuisance parameter - corresponding to the white noise component of the stellar activity - is added to the noise model of the likelihood function and is adjusted in the MCMC.

Regarding the Keplerian motion, we choose to adjust the natural log of the period and of the RV semi-amplitude to increase the efficiency of the MCMC due to the partial coverage of the orbit. We also probe the eccentricity and the argument of periastron through $\sqrt{e} \cdot \cos \omega$ and $\sqrt{e} \cdot \sin \omega$ variables. We use a uniform prior on these variables which also corresponds to a uniform prior in eccentricity and ω . The longitude of the ascending node, Ω , the inclination, i , and the relative orbit semi-major axis expressed in milli-arcseconds are also adjusted. The conversion from angles to AU is done using the GAIA parallax as a Gaussian prior. The orbit phase reference was chosen as the time at which the RV is minimum, T_{Vmin} , since it is well defined by the RV observations (see Fig.1).

We probe the full parameter space, composed of 16 parameters, using an MCMC with an adaptive Metropolis (Haario et al. 2001) and an adaptive scaling (Andrieu & Thoms 2008) which is particularly efficient at probing parameters with linear correlations. Additional tables and figures illustrating the results of the MCMC analysis are provided in the Appendix.

From combining the RV and direct imaging measurements we were able to bring good constraints on the geometry of the orbit and the mass of HD 13724 B. Based on the MCMC pos-

Table 3. Orbital elements of HD13724 B derived from the MCMC posterior distributions.

Param	Unit	Med	Std	CI(2.5%)	CI(97.5%)
P	yr	123	41	72	226
K	m/s	278	13	251	299
e		0.63	0.07	0.5	0.75
ω	deg	184.9	1.1	182.8	187.0
Ω	deg	16.4	4.2	7.3	23.9
i	deg	57.4	1.7	53.6	60.9
a_r	AU	26.3	5.6	18.3	39.5
T_{Vmin}	d ^(a)	56034	21	55993	56074
M_B	M_{Jup}	50.5	3.3	43.7	56.7

Notes. ^(a) The date is expressed as BJD-2400000.0.

terior distribution, we are able to set confidence intervals for the orbital elements and physical parameters of HD 13724 B. The 95% confidence interval for the period ranges from 72-226 yr, its semi-major axis between 18 and 40 AU and its mass between 43 and 56 M_{Jup} . Orbital elements values and confidence intervals are given in Table 3 while the full list of parameters adjusted in the MCMC is provided in the Appendix (Table A.1). The mass-period-eccentricity corner plot, based on the marginalised 2D posterior distribution is presented in Fig. 3 and illustrates the wide range of orbits still compatible with our data. However, the nature of HD 13724 B is without a doubt well below the hydrogen burning limit.

We note that these orbital solutions have higher eccentricities and longer periods than the one ones published in Rickman et al. (2019). This is explained by (1) the SPHERE measurements that rules out the shortest periods and (2) a significant improvement in our MCMC implementation that increase the efficiency to probe correlated parameter spaces (see Figure A.1).

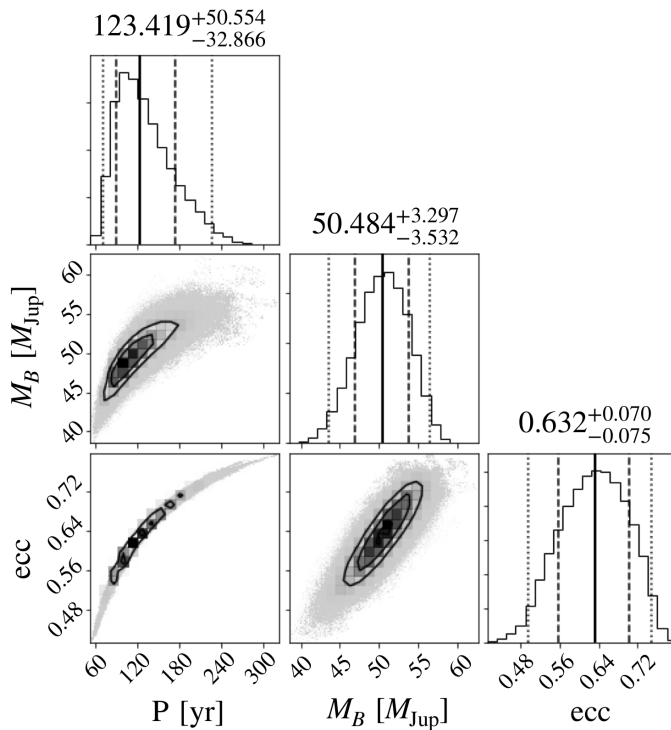


Fig. 3. Marginalised 1D and 2D posterior distributions of the orbital period, and eccentricity and the companion mass corresponding to the global fit of the RV and direct-imaging models. Confidence intervals at 2.275%, 15.85%, 50.0%, 84.15%, 97.725% are overplotted on the 1D posterior distributions, while the median $\pm 1\sigma$ values are given at the top of each 1D distribution. 1, 2 and 3 σ contour levels are overplotted on the 2D posterior distribution.

Table 4. The measured absolute photometry of HD 13724 B with the derived mass and temperature using Baraffe et al. (2003).

Band	App. Mag	Abs. Mag	Mass (M_{Jup})	Temp. (K)
H2	17.09 ± 0.16	13.90 ± 0.16	43.9 ± 1.8	1306 ± 48
H3	17.82 ± 0.32	14.63 ± 0.32	36.7 ± 3.0	1128 ± 74
J2	18.23 ± 0.40	15.04 ± 0.40	32.4 ± 4.0	1020 ± 99
J3	17.10 ± 0.05	13.91 ± 0.05	44.0 ± 0.6	1310 ± 18
K1	16.67 ± 0.18	13.48 ± 0.18	47.5 ± 2.2	1399 ± 56
K2	17.48 ± 0.46	14.29 ± 0.46	39.0 ± 4.3	1184 ± 106

4.3. Companion Properties

To allow a consistent comparison with other objects and to estimate the mass of HD 13724 B, we converted the $H2$, $H3$, $J2$, $J3$, $K1$ and $K2$ fluxes into absolute magnitudes using the *Gaia*-measured distance of HD 13724 (Gaia Collaboration et al. 2018) shown in Table 1. We then used the COND (Baraffe et al. 2003) substellar isochrones to predict the companion mass and temperature as a function of the calculated absolute photometry in each band. The resulting absolute photometric magnitudes, masses and temperatures are listed in Table 4.

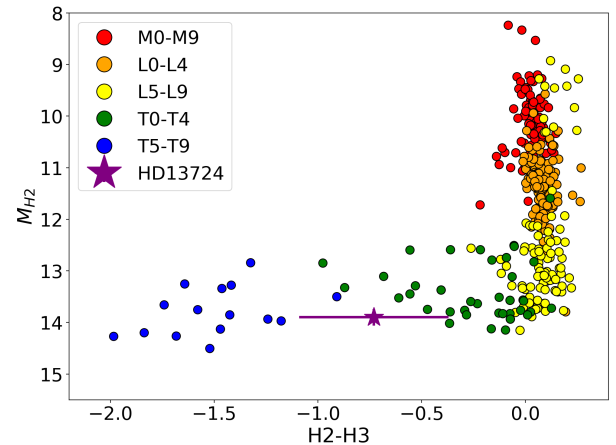


Fig. 4. Colour-magnitude diagram showing the predicted $H2$ - $H3$ colors and $H2$ absolute magnitudes for objects in the SpeX Prism Library (Burgasser 2014). The flux of HD 13724 B and the 1σ limit on its $H2$ - $H3$ color are shown. Its position is compatible with objects in the middle of the T sequence.

4.4. Spectral and atmospheric analysis

In order to estimate the spectral type of HD 13724 B, we used the SpeX Prism library of near-IR spectra of brown dwarfs (Burgasser 2014) using the *splat* python package (Burgasser et al. 2016) where each spectrum was flux calibrated to the distance of HD 13724. The *splat* package contains a library of observed brown dwarf spectra as well as theoretical models that we use as templates to derive the physical parameters.

Each SpeX Prism spectrum was also converted into the appropriate spectral resolution of each IFS measurement by convolution with a Gaussian. The FWHM used for the convolution was assumed to be $2x$ the separation between each wavelength channel. To fit the spectrophotometry of HD 13724 B with atmospheric models, we converted the contrast measurements into physical fluxes using a model spectrum for the host star ($T_{\text{eff}} = 5900$ K, $\log g = 4.5$ dex and $[\text{Fe}/\text{H}] = 0.3$ dex) from the BT-NextGen library (Allard et al. 2012) and the SPHERE filter transmission curves. The BT-NextGen spectrum is fit to the stellar energy distribution (SED) and is built using data from Tycho (Høg et al. 2000), 2MASS (Cutri et al. 2003), WISE (Cutri & et al. 2013) and HIPPARCOS (Perryman et al. 1997).

We calculated the χ^2_r of template brown dwarfs in the SpeX Prism library as a function of the spectral type. We include the uncertainties of the template spectra in the χ^2 computation. The best-fit object is 2MASS J10595185+3042059 (Cutri et al. 2003) which is classified as a T4 brown dwarf. In Fig. 5 we also plot the second best fit spectrum of SDSSp J092615.38+584720.9 (Cutri et al. 2003), which is classified as a T4.0/T4.5 brown dwarf. The temperatures of 2MASS J10595185+3042059 and SDSSp J092615.38+584720.9 are not given explicitly but effective temperatures of mid-T dwarfs covers a small range ($T_{\text{eff}} \approx 1100 - 1400$ K Kirkpatrick et al. (2000)). The T4 spectral type provides the best fit.

We use the $H2$ and $H3$ band values to place HD 13724 B on a colour-magnitude diagram as shown in Fig. 4 which is built using the SpeX Prism Library (Burgasser 2014). The placement of HD 13724 B on the colour-magnitude diagram agrees well with the estimated T spectral type.

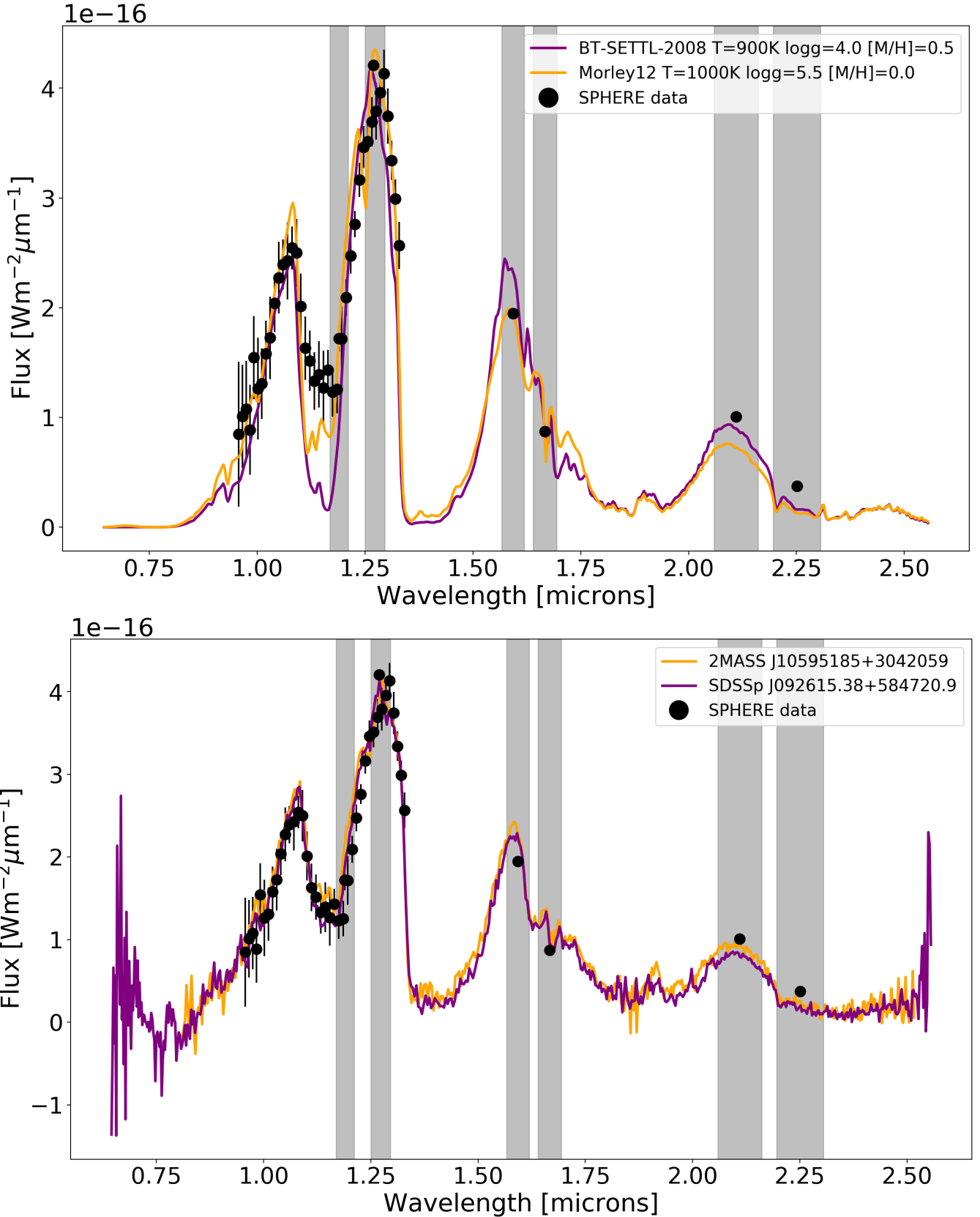


Fig. 5. Atmospheric spectra of HD 13724. The FWHM of the $J23$, $H23$ and $K12$ IRDIS filters are shown with grey bars (from left to right). The error bars on the $H2$, $H3$, $K1$ and $K2$ data are present but smaller than the size of the markers on each plot. **Top:** The two best-fitting spectra from BT-Settl 2008 models (Allard et al. 2012) and the Morley et al. (2012) models from the SpeX Prism library are overplotted, and the flux is scaled to match HD 13724 B. Fitting was performed to the IFS and IRDIS data simultaneously. **Bottom:** Comparison of the observed spectrum of HD 13724 B with the two best fit T4 brown dwarf atmospheres: 2MASS J10595185+3042059 and SDSSp J092615.38+584720.9 fitted using the *splat* package (Burgasser et al. 2016).

To further constrain the physical properties of HD 13724 B, we compared the observed spectral energy density to synthetic spectra for cool brown dwarfs from Morley et al. (2012) and Allard et al. (2012). The biggest difference between these models is that the Morley et al. (2012) models include the condensate sedimentation efficiency coefficients.

We adjusted the Morley et al. (2012) and the Allard et al. (2012) models, which sit well within the range of the mid-T dwarf range (see Fig. 5). The Morley et al. (2012) models are the best fit to the data with the following parameters of $T_{\text{eff}} = 1000$ K, $\log g = 5.5$ cm/s 2 , $f_{\text{SED}} = 3$, [M/H] = 0.0 and $R = 1.01 R_{\text{Jup}}$.

5. Summary and conclusions

In this paper we report the direct detection of a $\sim 50 M_{\text{Jup}}$ brown dwarf using VLT/SPHERE. HD 13724 B serves as an essential benchmark brown dwarf for testing brown dwarf atmospheric and evolutionary models where it joins just a short list of benchmark brown dwarf companions to stars with RV and imaging measurements: HR 7672 B (Liu et al. 2002; Crepp et al. 2012), HD 19467 B (Crepp et al. 2014), HD 4747 B (Sahlmann et al. 2011; Crepp et al. 2016; Peretti et al. 2019), GJ 758 B (Thalmann et al. 2009; Bowler et al. 2018), HD 4113 C (Cheetham et al. 2018), GJ 229 B (Nakajima et al. 1995; Brandt et al. 2019; Feng et al. 2020) and HD 72946 B (Maire et al. 2019).

We obtain images of HD 13724 B in the J , H and K bands along with its spectrum from IFS data in the $Y-J$ bands. Through comparison with the SpeX Prism Library of brown dwarf spectra (Burgasser 2014), we have found that HD 13724 B is most consistent with a spectral type of T4, which also agrees with the position of HD 13724 B on the $H2 - H3$ colour-magnitude diagram (Fig. 4). It should be noted that in general the template T4 brown dwarf provides a better fit than the synthetic spectra of Morley et al. (2012). This is especially true in the $K1$ and $K2$ bands where we observe more flux than what the models suggest. This might be due to clouds in the atmospheres that tend to increase the flux in the K -band (Marley et al. 1996; Morley et al. 2012). The template adjustment using the Morley et al. (2012) models allowed us to derive a temperature of 1000 K.

We analysed the HD 13724 system by combining RV measurements and high-contrast imaging, enabling us to place constraints on the orbital and physical parameters of HD 13724 B. This suggests a mass of $43-56 M_{\text{Jup}}$, an inclination of 53-60 deg and a period range of 72-226 years. We calculate the isochronal mass of HD 13724 B from the COND substellar isochrones (Baraffe et al. 2003) taking into account the age of the star. This gives a mass range of $31-52 M_{\text{Jup}}$ corresponding to an age of 0.5-2 Gyr. This overlaps with the mass range from the observations and suggests that either that the star is slightly older than expected or if the age is correct then some physics is missing from the modelling of the evolution of these substellar objects.

The combination of *Gaia* astrometry with future RV and imaging datasets will allow for much tighter constraints on the orbital and physical parameters of HD 13724 B, which in turn will improve the comparison with atmospheric and evolutionary models.

Many attempts have been made to detect these long period companions from the CORALIE RV survey through imaging as part of a 15-yr effort using VLT/NACO with little success. VLT/SPHERE is allowing us to now unveil these RV-detected brown dwarfs. We expect that the future upgrade of SPHERE (SPHERE+ Boccaletti 2019) will increase the sample

of cool brown dwarfs detected thanks to its higher contrast capabilities at short separations. Ultimately, future instruments like SPHERE+, the James Webb Space Telescope and the upcoming ELT/METIS (Carlomagno et al. 2016) should allow us to bridge the gap between the coolest brown dwarfs and the most massive giant planets.

Acknowledgements. This work has been carried out within the framework of the National Centre for Competence in Research PlanetS supported by the Swiss National Science Foundation. The authors acknowledge the financial support of the SNSF. This publications makes use of the The Data & Analysis Center for Exoplanets (DACE), which is a facility based at the University of Geneva (CH) dedicated to extrasolar planets data visualisation, exchange and analysis. DACE is a platform of the Swiss National Centre of Competence in Research (NCCR) PlanetS, federating the Swiss expertise in Exoplanet research. The DACE platform is available at <https://dace.unige.ch>. This work has made use of data from the European Space Agency (ESA) mission *Gaia* (<https://www.cosmos.esa.int/gaia>), processed by the *Gaia* Data Processing and Analysis Consortium (DPAC, <https://www.cosmos.esa.int/web/gaia/dpac/consortium>). Funding for the DPAC has been provided by national institutions, in particular the institutions participating in the *Gaia* Multilateral Agreement. This research has benefitted from the SpeX Prism Library (and/or SpeX Prism Library Analysis Toolkit), maintained by Adam Burgasser at <http://www.brown dwarfs.org/spexprism>. This research made use of the SIMBAD database and the VizieR Catalogue access tool, both operated at the CDS, Strasbourg, France. The original descriptions of the SIMBAD and VizieR services were published in Wenger et al. (2000) and Ochsenbein et al. (2000). This research has made use of NASA's Astrophysics Data System Bibliographic Services.

References

- Allard, F., Homeier, D., & Freytag, B. 2012, Philosophical Transactions of the Royal Society of London Series A, 370, 2765
- Amara, A. & Quanz, S. P. 2012, MNRAS, 427, 948
- Andrieu, C. & Thoms, J. 2008, Statistics and Computing, 18, 343
- Baraffe, I., Chabrier, G., Barman, T. S., Allard, F., & Hauschildt, P. H. 2003, A&A, 402, 701
- Baraffe, I., Homeier, D., Allard, F., & Chabrier, G. 2015, A&A, 577, A42
- Beuzit, J. L., Vigan, A., Mouillet, D., et al. 2019, arXiv e-prints, arXiv:1902.04080
- Boccaletti, A. 2019, in The Very Large Telescope in 2030, 38
- Boden, A. F., Torres, G., & Latham, D. W. 2006, ApJ, 644, 1193
- Bonnefoy, M., Lagrange, A. M., Boccaletti, A., et al. 2011, A&A, 528, L15
- Bowler, B. P., Dupuy, T. J., Endl, M., et al. 2018, AJ, 155, 159
- Brandt, T. D., Dupuy, T. J., Bowler, B. P., et al. 2019, arXiv e-prints, arXiv:1910.01652
- Burgasser, A. J. 2014, in Astronomical Society of India Conference Series, Vol. 11, Astronomical Society of India Conference Series
- Burgasser, A. J., Aganze, C., Escala, I., et al. 2016, in American Astronomical Society Meeting Abstracts, Vol. 227, American Astronomical Society Meeting Abstracts #227, 434.08
- Carlomagno, B., Absil, O., Kenworthy, M., et al. 2016, Society of Photo-Optical Instrumentation Engineers (SPIE) Conference Series, Vol. 9909, End-to-end simulations of the E-ELT/METIS coronagraphs, 990973
- Cheetham, A., Ségransan, D., Peretti, S., et al. 2018, A&A, 614, A16
- Crepp, J. R., Gonzales, E. J., Bechter, E. B., et al. 2016, ApJ, 831, 136
- Crepp, J. R., Johnson, J. A., Fischer, D. A., et al. 2012, ApJ, 751, 97
- Crepp, J. R., Johnson, J. A., Howard, A. W., et al. 2014, ApJ, 781, 29
- Cutri, R. M. & et al. 2013, VizieR Online Data Catalog, II/328
- Cutri, R. M., Skrutskie, M. F., van Dyk, S., et al. 2003, VizieR Online Data Catalog, II/246
- Delisle, J. B., Ségransan, D., Buchschacher, N., & Alesina, F. 2016, A&A, 590, A134
- Delisle, J. B., Ségransan, D., Dumusque, X., et al. 2018, A&A, 614, A133
- Dohlen, K., Langlois, M., Saisse, M., et al. 2008, in Proc. SPIE, Vol. 7014, Ground-based and Airborne Instrumentation for Astronomy II, 70143L
- Dupuy, T. J. & Liu, M. C. 2017, ApJS, 231, 15
- Ekström, S., Georgy, C., Eggenberger, P., et al. 2012, A&A, 537, A146
- Feng, F., Butler, R. P., Shectman, S. A., et al. 2020, arXiv e-prints, arXiv:2001.02577
- Gaia Collaboration, Brown, A. G. A., Vallenari, A., et al. 2018, A&A, 616, A1
- Gao, F. & Han, L. 2012, Computational Optimization and Applications, 51, 259
- Georgy, C., Ekström, S., Eggenberger, P., et al. 2013, A&A, 558, A103
- Haario, H., Saksman, E., & Tamminen, J. 2001, Bernoulli, 7, 223
- Hagelberg, J., Ségransan, D., Udry, S., & Wildi, F. 2016, MNRAS, 455, 2178

Hoeg, E., Bässgen, G., Bastian, U., et al. 1997, *A&A*, 323, L57

Høg, E., Fabricius, C., Makarov, V. V., et al. 2000, *A&A*, 355, L27

Kirkpatrick, J. D., Reid, I. N., Liebert, J., et al. 2000, *AJ*, 120, 447

Liu, M. C., Fischer, D. A., Graham, J. R., et al. 2002, *ApJ*, 571, 519

Maire, A. L., Baudino, J. L., Desidera, S., et al. 2019, arXiv e-prints, arXiv:1912.02565

Maire, A. L., Bonnefoy, M., Ginski, C., et al. 2016a, *A&A*, 587, A56

Maire, A.-L., Langlois, M., Dohlen, K., et al. 2016b, Society of Photo-Optical Instrumentation Engineers (SPIE) Conference Series, Vol. 9908, SPHERE IRDIS and IFS astrometric strategy and calibration, 990834

Mamajek, E. E. & Hillenbrand, L. A. 2008, *ApJ*, 687, 1264

Marley, M. S., Saumon, D., Guillot, T., et al. 1996, *Science*, 272, 1919

Marmier, M. 2014, PhD thesis, Geneva Observatory, University of Geneva, Switzerland

Mayor, M., Pepe, F., Queloz, D., et al. 2003, *The Messenger*, 114, 20

Mesa, D., Gratton, R., Zurlo, A., et al. 2015, *A&A*, 576, A121

Morley, C. V., Fortney, J. J., Marley, M. S., et al. 2012, *ApJ*, 756, 172

Nakajima, T., Oppenheimer, B. R., Kulkarni, S. R., et al. 1995, *Nature*, 378, 463

Ochsenbein, F., Bauer, P., & Marcout, J. 2000, *A&AS*, 143, 23

Pavlov, A., Möller-Nilsson, O., Feldt, M., et al. 2008, Society of Photo-Optical Instrumentation Engineers (SPIE) Conference Series, Vol. 7019, SPHERE data reduction and handling system: overview, project status, and development, 701939

Peretti, S., Ségransan, D., Lavié, B., et al. 2019, *A&A*, 631, A107

Perryman, M. A. C., Lindegren, L., Kovalevsky, J., et al. 1997, *A&A*, 323, L49

Queloz, D., Mayor, M., Naef, D., et al. 2000, in *From Extrasolar Planets to Cosmology: The VLT Opening Symposium*, ed. J. Bergeron & A. Renzini, 548

Rickman, E. L., Ségransan, D., Marmier, M., et al. 2019, *A&A*, 625, A71

Sahlmann, J., Ségransan, D., Queloz, D., et al. 2011, *A&A*, 525, A95

Santos, N. C., Israelian, G., & Mayor, M. 2001, *A&A*, 373, 1019

Santos, N. C., Sousa, S. G., Mortier, A., et al. 2013, *A&A*, 556, A150

Ségransan, D., Udry, S., Mayor, M., et al. 2010, *A&A*, 511, A45

Soummer, R., Aime, C., & Falloon, P. E. 2003, *A&A*, 397, 1161

Soummer, R., Pueyo, L., & Larkin, J. 2012, *ApJ*, 755, L28

Thalmann, C., Carson, J., Janson, M., et al. 2009, *ApJ*, 707, L123

Udry, S., Mayor, M., Queloz, D., Naef, D., & Santos, N. 2000, in *From Extrasolar Planets to Cosmology: The VLT Opening Symposium*, ed. J. Bergeron & A. Renzini, 571

Vigan, A., Bonnefoy, M., Ginski, C., et al. 2016, *A&A*, 587, A55

Vigan, A., Moutou, C., Langlois, M., et al. 2010, *MNRAS*, 407, 71

Wenger, M., Ochsenbein, F., Egret, D., et al. 2000, *A&AS*, 143, 9

Appendix A: MCMC results

Here we provide the full list of parameters adjusted in the MCMC as well as the marginalised 1D and 2D posterior distributions of the parameters corresponding to the global fit of the RV and direct-imaging models.

Table A.1. Parameters corresponding to the combined adjustment of the astrometric and RV observations of HD13724 AB derived from the MCMC posterior distributions.

Var	Units	Max(Proba)	Mode	Med	Std	CI(2.5%)	CI(97.5%)	Priors
M_\star	$[M_\odot]$							$N(1.14, 0.06)$
π	$[\text{mas}]$							$N(22.9781, \sqrt{0.0277^2 + 0.040^2})$
log (Proba)		-675.516	-685.396	-682.013	2.687	-688.373	-678.024	
$\gamma(H03)$	$[\text{m/s}]$	20833	20885	20806	36	20733	20870	U
$\Delta V(CVL - H03)^*$	$[\text{m/s}]$	-229	-303	-234	133	-496	27	$N(0, 300)$
$\Delta V(C98 - H03)$	$[\text{m/s}]$	-37.9	-35.8	-37.6	2.3	-42.2	-33.0	U
$\Delta V(C07 - H03)$	$[\text{m/s}]$	-37.8	-34.2	-41.0	4.5	-49.9	-32.2	U
$\Delta V(C14 - H03)$	$[\text{m/s}]$	-15.1	-21.2	-13.6	4.4	-22.3	-5.0	$N(-20, 5)$
S_{Act}	$[\text{m/s}]$	14.0	20.3	12.5	4.5	3.6	21.4	U
σ_J	$[\text{m/s}]$	7.03	7.17	7.11	0.62	5.98	8.39	U
log(P)	[day]	4.764	4.952	4.654	0.132	4.423	4.917	U
log(K)	$[\text{m/s}]$	2.459	2.483	2.444	0.020	2.400	2.476	U
$\sqrt{e} \cdot \cos \omega$		-0.827	-0.864	-0.792	0.043	-0.862	-0.702	U
$\sqrt{e} \cdot \sin \omega$		-0.070	-0.114	-0.067	0.014	-0.095	-0.039	U
$T_{V\text{min}}$	$[\text{bjd}]^{**}$	56033	56038	56034	21	55993	56074	U
Ω	[deg]	17.4	19.2	16.4	4.3	7.3	23.9	U
i	[deg]	58.5	58.6	57.40	1.7	53.6	60.0	U
a_r	$[\text{mas}]$	721	945	606	129	421	907	U
K	$[\text{m/s}]$	288	304	278	13	251	299	-
P	[y]	159	245	123	41	72	226	-
e		0.688	0.760	0.632	0.067	0.498	0.747	-
ω	[deg]	184.9	187.5	184.9	1.1	182.8	187.0	-
a_r	[au]	31.3	41.2	26.3	5.6	18.3	39.5	-
M_B	$[\text{M}_{\text{jup}}]$	53.1	56.3	50.5	3.3	43.7	56.4	-
$M_B, \sin(i)$	$[\text{M}_{\text{jup}}]$	45.3	48.1	42.5	3.5	35.3	48.6	-

*.: CVL stands for CORAVEL; **: The date is expressed as BJD-2400000.

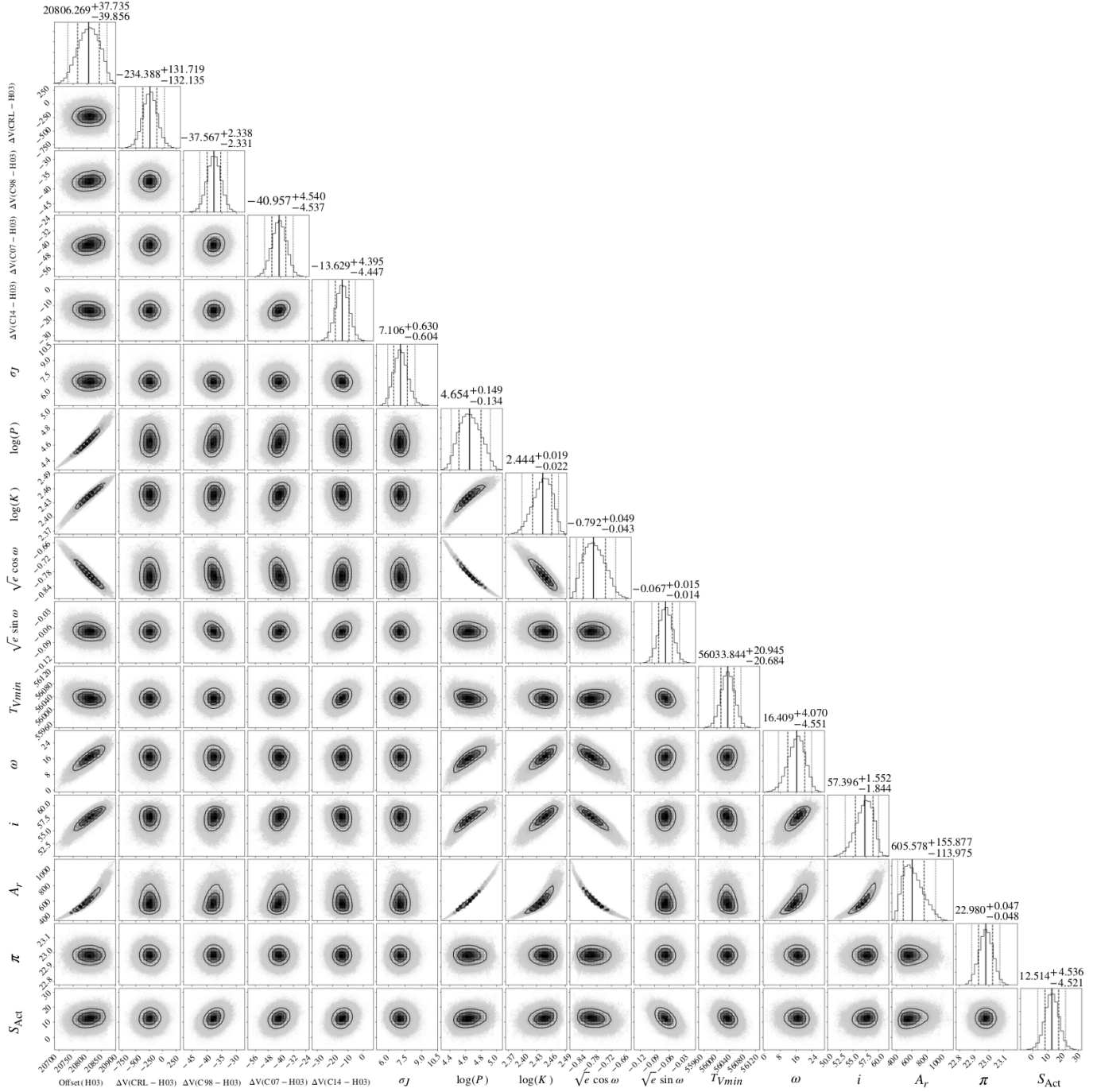


Fig. A.1. Marginalised 1D and 2D posterior distributions of the 16 parameters corresponding to the global fit of the RV and direct-imaging models. Confidence intervals at 2.275%, 15.85%, 50.0%, 84.15%, 97.725% are overplotted on the 1D posterior distributions, while the median $\pm 1 \sigma$ values are given at the top of each 1D distribution. 1, 2 and 3 σ contour levels are overplotted on the 2D posterior distribution. From left-to-right and top-to-bottom, the list of parameters are : $\gamma(H03)$, $\Delta V(CVL - H03)$, $\Delta V(C98 - H03)$, $\Delta V(C07 - H03)$, $\Delta V(C14 - H03)$, σ_J , $\log(P)$, $\log(K)$, $\sqrt{e} \cos \omega$, $\sqrt{e} \sin \omega$, $T_{V\min}$, i , ω , A_r , π , S_{Act} .